Review of Scientific Instruments ARTICLE scitation.org/journal/rsi

Circularly polarized microwave antenna for nitrogen vacancy centers in diamond

Cite as: Rev. Sci. Instrum. 91, 035003 (2020); doi: 10.1063/1.5129863
Submitted: 2 October 2019 • Accepted: 22 February 2020 •
Published Online: 17 March 2020

Vitaly Yaroshenko,[1] Vladimir Soshenko,[2] Vadim Vorobyov,[2,3] Stepan Bolshedvorskii,[2,4] Elizaveta Nenasheva,[5] Igor Kotel'nikov,[6] Alexey Akimov,[2,7,8] and Polina Kapitanova[1,a)]

AFFILIATIONS

[1]Department of Physics and Engineering, ITMO University, 197101 Saint Petersburg, Russia
[2]P. N. Lebedev Physical Institute, 119991 Moscow, Russia
[3]Institute of Physics and Center for Applied Quantum Science, University of Stuttgart, 70550 Stuttgart, Germany
[4]Moscow Institute of Physics and Technology, 141700 Moscow Region, Russia
[5]Ceramics Co., Ltd., 10, Kurchatova St., Saint Petersburg 194223, Russia
[6]Saint Petersburg Electrotechnical University "LETI", 5, Popova St., Saint Petersburg 197356, Russia
[7]Russian Quantum Center, 143025 Moscow, Russia
[8]Texas A&M University, College Station, Texas 77843, USA

[a)]**Author to whom correspondence should be addressed:** p.kapitanova@metalab.ifmo.ru

ABSTRACT

The sensing applications of nitrogen-vacancy color centers in a diamond require an efficient manipulation of the color center ground state over the whole volume of an ensemble. Thus, it is necessary to produce strong uniform magnetic fields of a well-defined circular polarization at microwave frequencies. In this paper, we develop a circularly polarized microwave antenna based on the excitation of hybrid electromagnetic modes in a high-permittivity dielectric resonator. The influence of the geometrical parameters of the antenna on the reflection coefficient and magnetic field magnitude is studied numerically and discussed. The Rabi frequencies and their inhomogeneity over the volume of a commercially available diamond sample are calculated. With respect to the numerical predictions, a Rabi frequency as high as 34 MHz with an inhomogeneity of 4% over a 1.2 mm × Ø2.5 mm (5.9 mm^3 in volume) diamond sample can be achieved for 10 W of input power at room temperature. The antenna prototype is fabricated, and experimental investigations of its characteristics are performed in microwave and optical frequency domains. The circular polarization of the microwave magnetic field with an ellipticity of 0.94 is demonstrated experimentally. The Rabi oscillation frequency and its inhomogeneity are measured, and the results demonstrate a good agreement with the numerically predicted results.

I. INTRODUCTION

Development of sensors based on nitrogen-vacancy (NV) color centers is very promising for the observation of brain activity, the accurate detection of neuronal activity related to muscle control, high-precision monitoring of temperature, for example, in bioapplications, and detecting small changes in the amplitude of the (DC) magnetic field of the Earth.[1–6] The magnetic field sensor's sensitivity can be enhanced by the application of a large ensemble of NV centers,[5,7,8] which normally occupy only one of four possible orientations,[9,10] hence, leading to a reduction in the optically detected magnetic resonance (ODMR) contrast by a factor of 4. Recently, preferentially oriented ensembles of NV centers were demonstrated.[11–13] It was shown that 99% of the NV centers were oriented along the ⟨111⟩ crystallographic axis, which in such cases is perpendicular to the main surface of the diamond plate sample. As a result, it was capable of having a full contrast of approximately 30% for a single orientation, producing a factor of 4 improvement in the magnetic field sensitivity.[14,15] Such diamond samples could be used to enhance the fluorescence contrast in 3D ensemble and shallow 2D ensemble experiments, possibly with the addition of a wide-field magnetometry technique.[16,17] However, for such NV ensembles,

efficient microwave (MW) control would require a uniform over a large volume transverse MW magnetic field perpendicular to the ⟨111⟩ axis in the plane with the diamond surface. In addition, the use of a circularly polarized instead of a linearly polarized MW field opens a way to selectively address single transitions in cases where transitions overlap at a very low magnetic field. For example, a circularly polarized MW drive for NV centers was recently used in zero-field nuclear magnetic resonance (NMR) experiments.[18] Notably, the use of circular polarization allows one to minimize the level of MW power by a factor of $\sqrt{2}$. An increase in the utilized NV ensemble volume is another key to improve diamond magnetometer sensitivity.[15,17] Thus, the microwave field inhomogeneity provided by an antenna over the exposed diamond volume becomes a figure of merit for NV ensemble manipulation.

Different designs of MW antennas for the manipulation of the spins of NV centers in the diamond have been proposed and studied experimentally. Among them are wire design,[19] planar double split ring antenna,[20] planar ring antenna,[21] microstrip antenna,[22] and macroscopic dielectric microwave cavity.[23] Most of the described antennas generate a uniform magnetic field with linear polarization in a small area of 1 mm^2. However, to improve the sensitivity and precision of a sensor, the microwave field should be generated efficiently over a large volume. For this purpose, a loop gap resonator,[7] dielectric resonator antenna,[8,24] and metallic cavity[23,25] have been proposed. Nevertheless, none of these designs realize an in-plane microwave field with circular polarization and low inhomogeneity over a large volume.

In this paper, we propose the design of an antenna with a circularly polarized, uniform magnetic field over a large volume for the coherent and effective spin manipulation of NV centers as shown in Fig. 1. We demonstrate that the proposed antenna can potentially be used for the efficient control of an NV center spin ensemble over the whole volume of a commercially available diamond sample. We provide numerical and experimental results of the antenna's characteristics, including the reflection coefficient, magnetic field magnitude, ellipticity, and Rabi frequency and its inhomogeneity over a chosen volume.

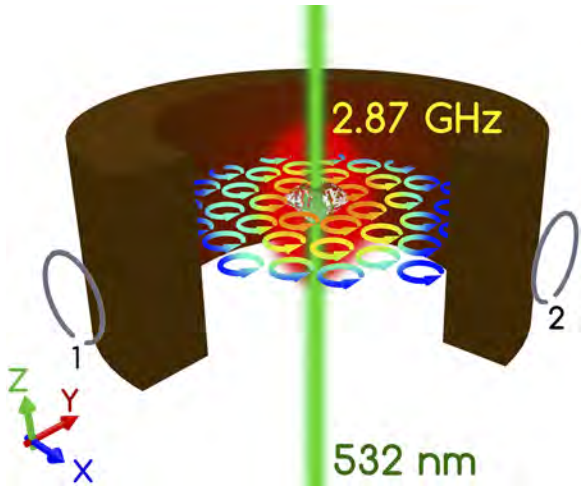

FIG. 1. Artist view of the DRA, which consists of a hollow cylindrical dielectric resonator excited by two loops. An optical sample containing NV centers is placed at the center of the resonator bore and pumped by using a green laser.

II. DRA DESIGN AND RESULTS OF THE NUMERICAL SIMULATIONS

A. DRA operational principle and design

The operational principle of the antenna design is based on the excitation of two orthogonal $HEM_{11\delta}$ modes inside a hollow cylindrical dielectric resonator [see Fig. 1]. To obtain a circular polarization, the modes must be excited with signals of the same amplitude and a 90° phase difference.

Empirical expressions for the estimation of the resonance frequencies of the lowest modes of a cylindrical dielectric resonator have been derived[26,27] and can be used to estimate the frequency of the $HEM_{11\delta}$ mode,

$$f_{HEM_{11\delta}} = 2.735\frac{c\varepsilon^{-0.436}}{2\pi R}\left[0.543 + 0.589\frac{R}{T} - 0.05\left(\frac{R}{T}\right)^2\right], \quad (1)$$

where c is the speed of light, R is the resonator's radius, T is the resonator's height, and ε is the permittivity of the dielectric material. Using Eq. (1), we calculated the resonance frequency of the $HEM_{11\delta}$ mode for different values of the dielectric resonator permittivity and height when the radius is fixed [see Fig. 2(a)]. There are many degrees of freedom that can be employed to achieve a resonance frequency of 2.87 GHz, which is equal to the zero-field splitting of the ODMR of the NV center for a given permittivity and height of the resonator.

Usually, natural dielectric materials do not possess high-permittivity in the microwave frequency range.[28]

For MW applications, it is convenient to use MW ceramics, which can be synthesized to achieve a high-permittivity with a low dielectric loss and temperature coefficient.[28,29] In the current study, we consider a MW ceramic with a permittivity of ε = 235 and a dielectric loss tangent of tan(δ) = 0.003 measured at 3 GHz.[29] The dependence of the $HEM_{11\delta}$ mode frequency as a function of resonator height for different radii calculated by means of Eq. (1) is shown in Fig. 2(b). Following the obtained results, one can estimate the dielectric resonator dimensions as a radius of R = 3.95 mm and a height of T = 5.52 mm for the $HEM_{11\delta}$ mode at 2.87 GHz.

B. Numerical optimization of the DRA

Next, we perform numerical simulations of the dielectric resonator antenna (DRA) performances using the frequency domain solver of CST Studio Suite. The feeding loops are used to excite the dielectric resonator. They are identical in size, have a radius of 2 mm, and a wire size of 0.25 mm. They are located at the center of the resonator, 0.5 mm from the surface and 90° apart from each other (see Fig. 1). MW ports with a 50 Ω impedance are placed in the 2 mm gap of the loops. To obtain the circular polarization of the DRA, two orthogonal $HEM_{11\delta}$ modes are excited with a 90° phase difference between the signals at ports 1 and 2. A resonator permittivity of ε = 235 and the dimensions previously estimated by Eq. (1) are used. However, the ceramic resonator now has an entire bore to place an optical sample (diamond plate with NV centers) inside. The size of the resonator with the bore taken into account has been

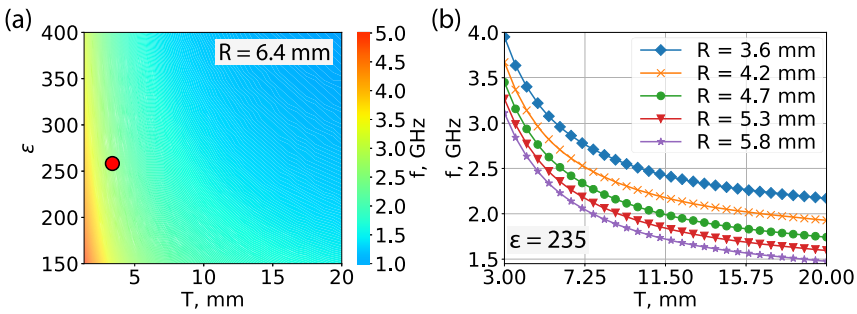

FIG. 2. (a) Frequency of the $HEM_{11\delta}$ mode excited in the dielectric resonator as a function of resonator's height and permittivity for a fixed radius calculated by using Eq. (1). The red point shows the measured permittivity for the DRA with a bore. (b) Dependence of the $HEM_{11\delta}$ mode frequency as a function of resonator's height for different values of the radius with $\varepsilon = 235$.

optimized numerically in CST Studio Suite to excite the $HEM_{11\delta}$ mode at 2.87 GHz. After the optimization of the DRA with a bore radius of $R_{in} = 1.6$ mm, we obtained an outer radius of $R = 3.95$ mm and a height of $T = 6.2$ mm. The simulated return loss of the DRA has a minimum at 2.87 GHz [see Fig. 3(a)].

The important parameter that affects the DRA reflection coefficient and magnetic field magnitude is the dielectric loss of the ceramic material. Initially, we consider the level of the dielectric loss tangent as $\tan(\delta) = 3 \times 10^{-3}$ with an MW magnetic field amplitude of 720 A/m at 5 W (total of 10 W) for the input power of each input port [see Figs. 3(b) and 3(d)]. However, the level of the dielectric loss of the ceramic can slightly deviate from this value. Thus, it is important to estimate its impact on the DRA performance. With respect to the results of the numerical simulations, increasing the dielectric loss value leads to a degradation in the MW magnetic field amplitude in the DRA center [see Fig. 3(a)]. For a dielectric loss tangent of $\tan(\delta) = 5 \times 10^{-3}$, the amplitude of the MW magnetic field in the DRA center decreases to 630 A/m for an input power of 5 W for each input

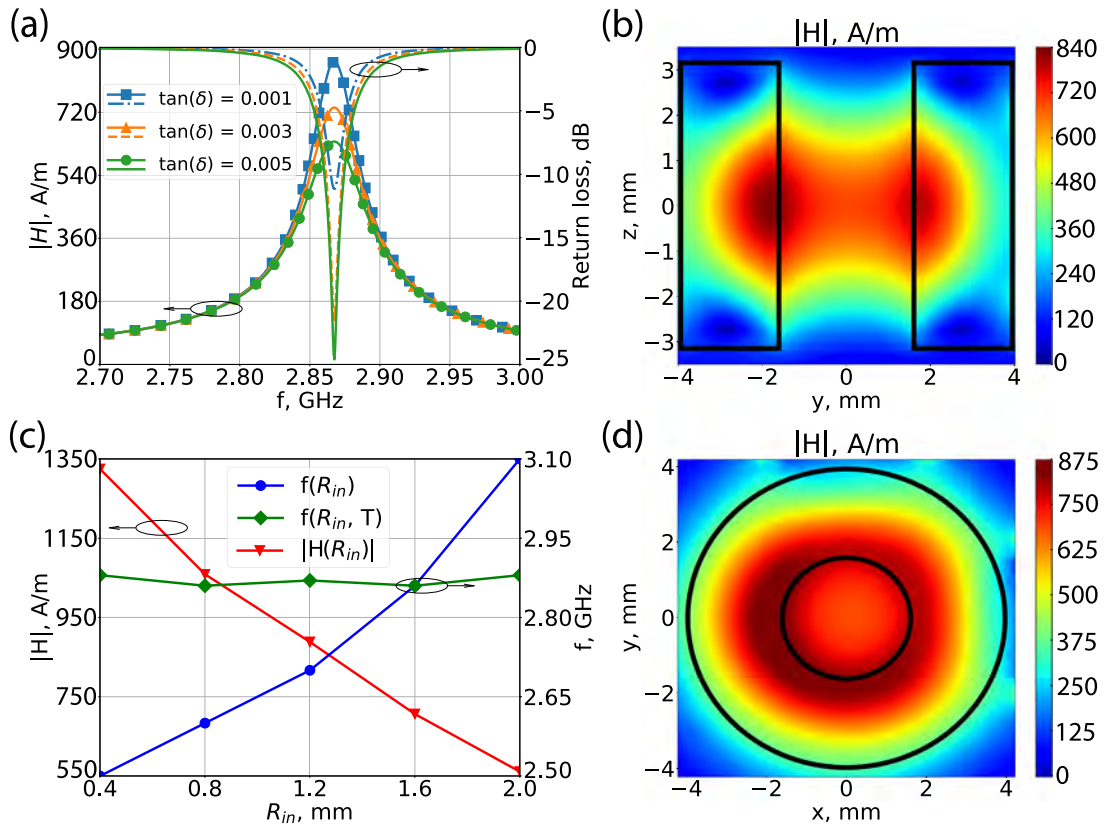

FIG. 3. (a) Simulated return loss and magnitude of the MW magnetic field of the DRA for different values of the dielectric loss tangent. A simulated magnitude of the MW magnetic field in the y–z (b) and x–y (d) planes of the DRA at 2.87 GHz. (c) Simulated resonance frequency and magnitude of the MW magnetic field of the DRA as a function of entire bore radius. The resonance frequency is determined at the minimum of the return loss. The magnitude of the MW magnetic field is taken at the center of the resonator's bore.

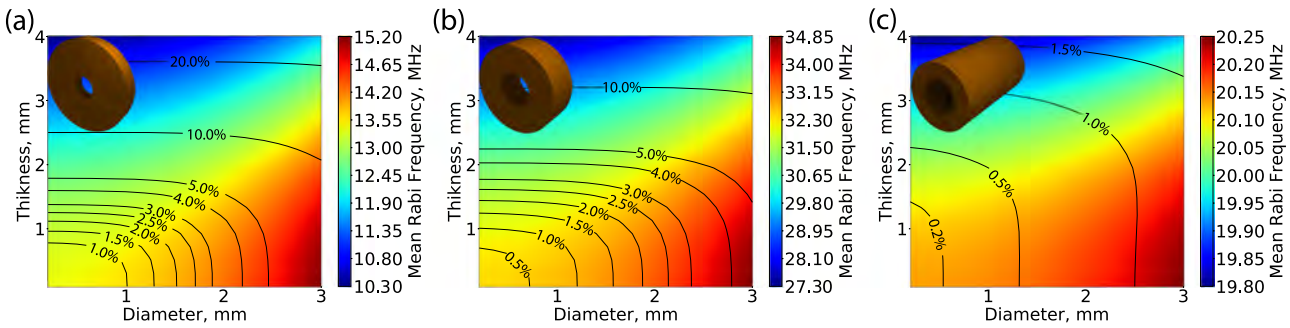

FIG. 4. Mean value and inhomogeneity (isolines) of the Rabi frequency simulated over the diamond volume for the DRA designs with the geometrical ratio of the resonator's radius and height $2R \gg T$ (a), $2R \approx T$ (b), and $2R \ll T$ (c), which are shown by insets for illustrative purposes. The Rabi frequency values are obtained for a total input power of 10 W.

port. The reflection coefficient is better than −15 dB. On the other hand, if the level of the dielectric loss tangent is on the order of $\tan(\delta) = 1 \times 10^{-3}$, then the MW magnetic field is approximately 900 A/m, but the DRA return loss is not better than −10 dB. The optical sample would be placed at the center of the resonator bore since the MW magnetic field is localized inside the DRA [see Figs. 3(b) and 3(d)]. As the hole radius of the DRA increases, we observe an increase in the resonance frequency and a decrease in the magnitude of the MW magnetic field in the center of the DRA [see Fig. 3(c)]. However, the resonance frequency can be kept at approximately 2.87 ± 0.01 GHz by optimizing the antenna height.

C. Rabi frequency estimation

To understand the achieved MW magnetic field level inside the dielectric resonator, one could estimate the Rabi oscillation frequency of the NV center spin ensemble. Normally, this value is less than 10 MHz for a relatively low power level of 5 W.[8,20,22,30] In the case of a circularly polarized MW magnetic field, the Rabi frequency can be calculated as[31]

$$\Omega = 2\gamma_e |\langle 0|\hat{S}_x|1\rangle| B = \sqrt{2}\gamma_e B, \tag{2}$$

where $\hat{S}_x$ is the spin projection operator on the x-axis, B is the magnetic field, and γ_e is the gyromagnetic ratio. A factor of 2 appears when a field with circular polarization is utilized. Equation (2) gives the value of the Rabi frequency at one specific point, but for the case of a bulk diamond, it is very important to estimate the mean value and deviation of the Rabi frequency. The deviation provides information about the inhomogeneity of the MW magnetic field, which affects the precision of NV-based sensors. In this case, the following equation, where the Rabi frequency is integrated over the diamond volume, can be used:

$$\langle \Omega \rangle = \frac{\int_V \Omega dV}{\int_V dV}, \tag{3}$$

where V is the diamond volume. The standard deviation of the mean value of the Rabi frequency can be given as

$$\langle \sigma \rangle = \sqrt{\left(\frac{\int_V \Omega dV}{\int_V dV}\right)^2 - \left(\frac{\int_V \Omega^2 dV}{\int_V dV}\right)}. \tag{4}$$

Using Eqs. (2)–(4) and simulated MW magnetic field distribution, we estimated the mean value and average deviation of the Rabi oscillation frequency. For simplicity, we suppose that the diamond sample has a cylindrical shape and characterizes by diameter and thickness. The numerically obtained mean values of the average deviations of the Rabi oscillation frequency vs the volume of the diamond results for the DRA with the parameters described above are shown in Fig. 4(b). Now, the DRA has the diameter which is comparable to the height (2R ≈ T). For such a design, we found that over the 1.2 mm × Ø2.5 mm diamond sample (5.9 mm^3 in volume), a mean Rabi frequency of 34 MHz with an inhomogeneity of 4% can be achieved for 10 W of total input power [see Fig. 4(b)]. The effect of this 4% inhomogeneity on a magnetometer performance could be understood using data from Ref. 32. The 4% inhomogeneity corresponds to a uniformity of 96.5% and gives additional 1% sensitivity error. Two additional DRA designs with the geometries 2R ≫ T and 2R ≪ T have been numerically studied. For the first additional design, we drastically reduced the height and increased the radius (2R ≫ T), leading to the following geometrical parameters: R = 6.4 mm and T = 4.24 mm. For this design, we observe a mean Rabi frequency of 14.5 MHz and an inhomogeneity of 6% over the same volume [see Fig. 4(a)]. For the second design, we did the opposite, keeping the radius much smaller than the height (2R ≪ T): R = 2.9 mm and T = 18.5 mm. We find that the mean value of the Rabi frequency reaches 20 MHz with an inhomogeneity of 1% [see Fig. 4(c)]. Note that the bore radius has been kept the same (R_{in} = 1.6 mm) for all designs. One may conclude that the optimal design in terms of mean Rabi frequency and inhomogenity is the design with a comparable diameter and height of the dielectric resonator $2R \approx T$. If a desired application is somehow limited in terms of DRA height but does not require a large Rabi frequency, then one can choose a DRA with the following ratio of the geometrical parameters: 2R ≫ T. In contrast, when a high homogeneity is needed, one must choose the design that satisfies the following condition: 2R ≪ T.

III. EXPERIMENTAL STUDY

A. DRA prototype

A DRA with the large-radius geometry (2R ≫ T) was chosen for prototyping and an experimental study. Initially, the permittivity

of microwave ceramics based on a mixture of $BaTiO_3/SrTiO_3$ with Mg-containing additions[29] available for dielectric resonator fabrication was investigated. The composition and concentration of Mg-containing additions influence the ceramic permittivity and loss tangent. Thus, these values for a set of test dielectric resonators were measured by means of two different techniques for rectangular[33] and cylindrical[34] resonator shapes. The measured permittivity of $\varepsilon = 254$ and the dielectric loss tangent of $\tan(\delta) = 2.7 \times 10^{-3}$ are obtained at a frequency of 3 GHz and are shown by the red dot in Fig. 2(a). A slight deviation of the measured value from the numbers used for the numerical simulations must be taken into account during the DRA prototype optimization.

To obtain a clear experimental picture excluding any beat signals, we preferred to measure the Rabi frequency of a single NV center orientation. The easiest way to perform this measurement is to detune the selected orientation of the NV center with the help of a bias magnetic field. Thus, the resonance frequency of the DRA prototype has to be optimized for the frequency range of 2.65–2.68 GHz.

To develop a DRA prototype that is compatible with a printed circuit board (PCB) technology, we changed the excitation type. Here, we used two 50 Ω microstrip lines instead of the loops.[26,27] The influence of the excitation method on the DRA performance was numerically studied.[35] We found that this excitation method practically does not affect the DRA mode and provides only a slightly (no more than 9%) smaller field amplitude for a given power of 10 W.

Considering the measured permittivity value, a new type of excitation, and the desired MW frequency range, the DRA was numerically optimized, and new dielectric resonator dimensions were obtained as follows: $T = 4.24$ mm, $R = 6.4$ mm, and $R_{in} = 1.5$ mm. The excitation network of the DRA prototype [see Fig. 5(a)] was implemented using a 1.5-mm-thick FR-4 substrate with dimensions of 45 mm × 45 mm. The length of the 50 Ω microstrip lines was 20 mm. The dielectric resonator was fixed by glue in the middle of the substrate.

The simulated return loss of the DRA prototype is better than −10 dB in the desired frequency range, as shown in Fig. 5(b). Due to the asymmetric position of the feeding microstrip lines with respect to the dielectric resonator center along the z direction, the magnetic field distribution inside the DRA changes [see Fig. 5(c)]. Now, the maximum of the MW magnetic field is shifted closer to the PCB. It is important to take this shift into account when positioning an optical sample during the experimental study. From the simulated results, one can predict that the sample should be shifted by approximately 1 mm down in the z direction from the center of the DRA.

B. Measured results

The return loss of the DRA was experimentally studied in the microwave frequency range by connecting the DRA to the ports of an E8362C PNA microwave network analyzer. From Fig. 5(b), one can see that both ports of the DRA are matched better than −10 dB in the frequency range of 2.65–2.68 GHz.

An experimental study of the NV center fluorescence emission was conducted with the help of a home-built microscope with an external microwave part. The setup is shown in Fig. 6(a). As a basic sensitive element, a 1.2 × 1.2 × 0.3 mm^3 diamond plate with a 14.6 ppm NV concentration cut perpendicular to the ⟨111⟩ orientation was used.[36] The diamond plate was fixed onto a sapphire cylinder 2 mm in diameter and placed inside the DRA. The ⟨111⟩ orientation of the diamond lattice was oriented along the z axis of the dielectric resonator and along the optical axis of the microscope objective lens. Both the diamond plate and the DRA were connected to XYZ stages to control their position with respect to each other and to the microscope objective lens. A continuous-wave laser (Coherent Compass 300, wavelength of 532 nm) was served as a source for the NV center excitation. To perform the pulsed experiments, an acousto-optic modulator (AOM) was utilized for an on–off modulation of the optical pumping. Imaging was realized with the help of galvo mirrors (Cambridge Technologies). An Olympus 10× Plan Achromat objective lens with a numerical aperture of NA = 0.25 and a working distance of 10.6 mm was used to focus the excitation and collect the emission from the diamond. The collected fluorescence was coupled into an avalanche photodiode (PerkinElmer SPCM-AQRH-14-FC). We used a combination of an optical notch filter with a stop band centered at 532 nm and a longpass optical filter with a cutoff at 600 nm to remove the residual green excitation light and Raman signal from the collected emission. The bias magnetic field was created using a permanent magnet, which was placed next to the DRA to split the ODMR position and choose only one of four possible orientations for the Rabi frequency measurements. This was achieved by placing the magnet aligned with respect to the diamond's ⟨111⟩ crystallographic axis and creating the field along the ⟨111⟩ axis.

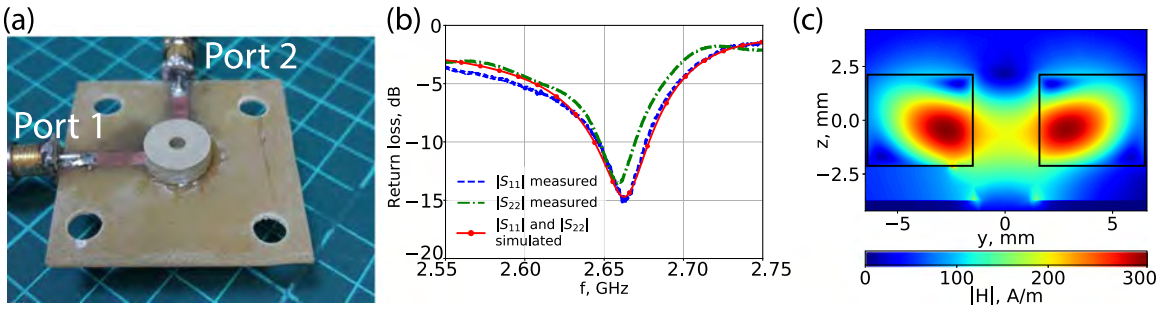

FIG. 5. (a) Photograph of the DRA prototype. (b) Simulated and measured return losses of the DRA. (c) The simulated MW magnetic field distribution inside the DRA obtained for 2 W of power at each DRA input port.

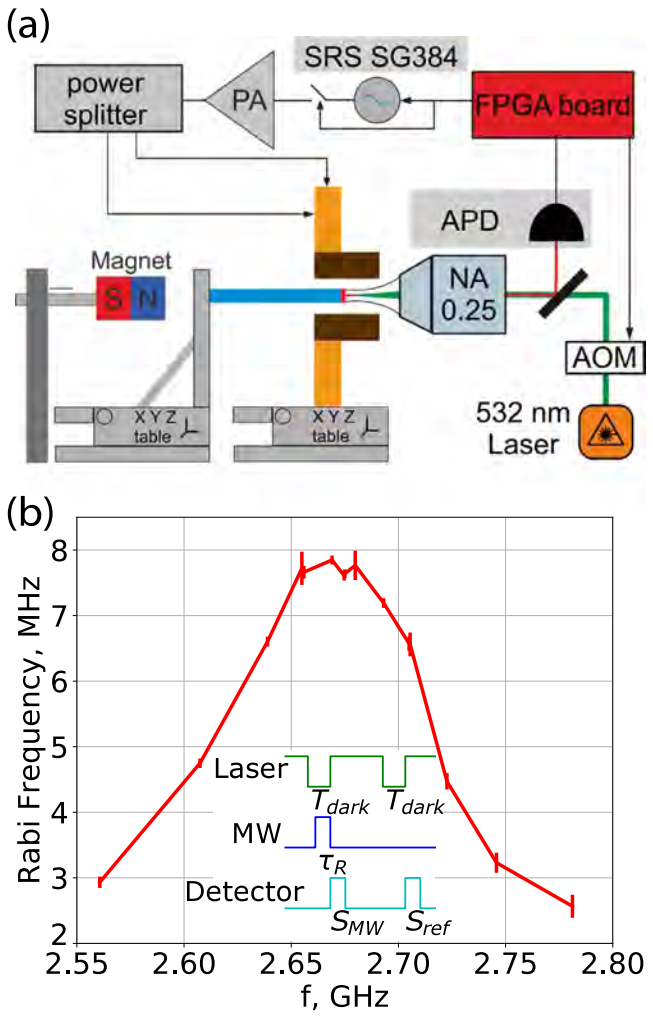

FIG. 6. (a) The experimental setup. (b) Dependence of the measured Rabi frequency on the MW frequency. The inset shows the pulse sequences used for the Rabi oscillation measurements.

To deliver the MW signal to the DRA, we used a Stanford Research System SG384 signal generator modulated by using a Mini-Circuits ZASWA-2-50DR switch and amplified by using a Mini-Circuits ZHL-16W-43+ power amplifier. Power splitters (Mini-Circuits ZX10Q-2-34-S+ and Mini-Circuits ZX10-2-332-S+) were used to equally divide the signal amplitude. The change in the power splitter provided the desired phase difference (+90°, −90°, or 0°) between the input ports of the DRA. A National Instruments PCIe-7851 FPGA card was used to produce control pulses for optical and microwave pumping. The Avalanche Photodiode (APD) counting and gating were implemented internally in the card.

We started the experimental investigation with measurements of the Rabi frequency dependence inside the DRA. To measure the Rabi oscillations, we varied the pulse duration and measured the number of counts at two different times: after the spin polarization with green light but before the application of the MW pulse (S_{ref}) and right after the MW pulse (S_{MW}) [see the inset in Fig. 6(b)]. Thus, the spin contrast can be calculated as $C = (S_{MW} - S_{ref})/(S_{ref} + S_{MW})$.

First, we experimentally found the z coordinate with the maximum of the MW magnetic field. For this purpose, we placed the diamond plate at the center of the DRA ($x = y = z = 0$) and moved the DRA along the z direction, measuring the Rabi oscillations at a MW frequency of 2.66 GHz. We found this value to be $z = -0.95$ mm. The DRA operation frequency range was measured next. The diamond plate was positioned in the maximum of the MW magnetic field inside the DRA ($x = y = 0$, $z = -0.95$ mm). By tuning the bias magnetic field, the resonance position of the NV center electron spin changed. The Rabi oscillations were detected for each bias magnetic field magnitude. The obtained frequency dependence is depicted in Fig. 6(b). A maximum Rabi frequency of 7.8 MHz was achieved at

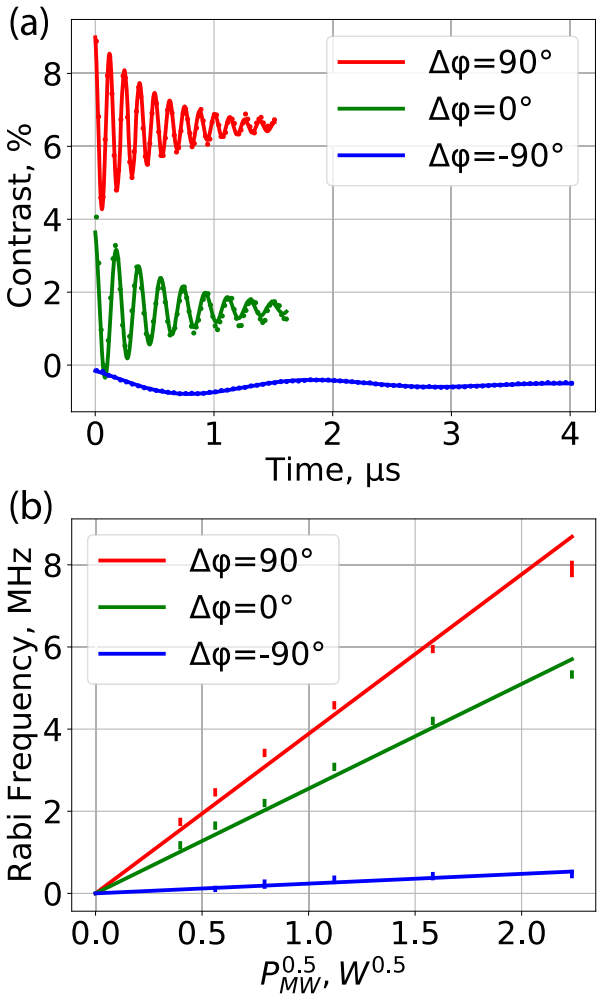

FIG. 7. (a) Rabi oscillations for different phase shifts in the input ports of the DRA. Offsets of 5% (green line) and 10% (red line) are added for illustrative purposes. (b) Dependence of the Rabi oscillation on $\sqrt{P_{MW}}$ for different phase shifts in the input ports of the DRA.

an MW frequency of 2.67 GHz. The estimated bandwidth of the resonance peak (full width at half maximum) is 140 MHz.

Next, we investigated the polarization of the MW field generated by the DRA using the Rabi oscillation measurement technique described by Herrmann *et al.*[30] The diamond plate was positioned in the maximum of the MW magnetic field inside the DRA (x = y = 0, z = −0.95 mm), and the NV resonance was tuned to 2.67 GHz. The measured spin contrasts at $\Delta\varphi = 0^\circ$ and $\pm 90^\circ$ under the same MW power are shown in Fig. 7(a). The measured Rabi oscillations as a function of MW signal power are plotted in Fig. 7(b). The linear relation between the Rabi frequency and the square root of the MW power, which is generally expected for Rabi oscillation experiments,[30] is verified for all phase shifts. The two slopes in Fig. 7(b) of 3.88 ± 0.04 MHz/$\sqrt{\text{W}}$ for $\Delta\varphi = 90^\circ$ and 0.23 ± 0.03 MHz/$\sqrt{\text{W}}$ for $\Delta\varphi = -90^\circ$ provide an ellipticity of 0.94. Therefore, the circular polarization of the magnetic field is confirmed experimentally.

Finally, we experimentally studied the Rabi frequency distribution provided by the DRA in the central cross section over the XY plane. The diamond plate was fixed in the maximum of the magnetic field inside the DRA, directly in the microscope focus. The investigation was done with the help of galvo mirrors enabling 0.8 mm × 0.8 mm field of view for the microscope on the grid of 5 × 5 pixels. At each pixel, the full Rabi oscillations were measured with a pulse time sweep over a narrow MW frequency band. The frequency band was 10 MHz near the NV resonance frequency with a 0.5 MHz time step. The pulse time was swept from 12.5 ns to 600 ns with a 12.5 ns time step. Resulting data were fitted with the 2D Rabi oscillation model, regarding all three hyperfine components. Frequency sweep was intended to exclude detuning effects due to the DC magnetic field gradient and strain distribution in the crystal. From the measured data, it was found that the NV resonance frequency deviated within ±0.3 MHz, corresponding to the constant magnetic field deviation of ±8 A/m in the scanned area. The measured Rabi frequency distribution map is compared to the numerically obtained map in Fig. 8. A good agreement between the measured data and simulated results is observed. A minimum Rabi frequency value of 7.13 MHz was measured in the middle of the scanning area. A maximum Rabi

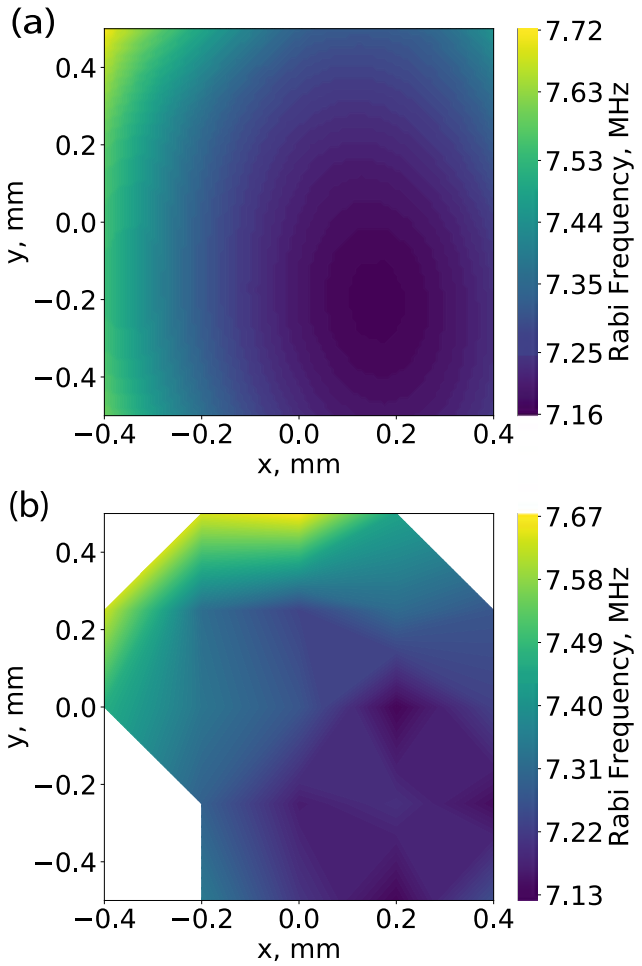

FIG. 8. (a) Simulated and (b) measured Rabi frequency distribution maps obtained in the middle of the DRA ($x = y = 0$, $z = -0.95$ mm). The simulated results and measured data were obtained for 2 W of input power at each port of the DRA.

TABLE I. The MW antennas' performances.

Design	References	MW polarization	MW input power (W)	Rabi frequency (MHz)	Rabi frequency (MHz/$\sqrt{\text{W}}$)	Bandwidth (MHz)	Diamond sample (mm^3)	Inhomogeneity, % over the area/volume (mm^2/mm^3)
MW circuit	22	Linear/circular	0.04	1.2/1.57	1.6/2.05	Non-resonant	3 × 3 × 0.5	. . .
Planar SRR	20	Linear	0.5	16.69	23.6	40	3 × 3 × 0.5	4.4 (1.14/-)
Microwave circuit	30	Linear/circular	3.33	1.1/1.46	0.6/0.8	165	2.5 × 2.5 × 0.5	. . .
Planar ring antenna	21	Linear	1	4.6	4.6	400	2.2 × 2.2 × 0.51	. . .
DRA	8	Linear	5.2	10	4.3	30	1.2 × 1.2 × 0.3	1 (-/5.9)
LGR	7	Linear	16	7.7	1.9	80	4.5 × 4.5 × 0.5	1.6 (11/-)
DRA	Current design	Circular	4	7.87	2.6/3.9	140	1.2 × 1.2 × 0.3	4(-/5.9)

frequency value of 7.67 MHz was achieved at the edges of the scanning area. Thus, the peak-to-peak Rabi frequency change in the XY plane over a scanned area of 0.8 mm^2 is 0.54 MHz with a standard deviation of 0.16 MHz as estimated by Eq. (4).

We carried out two types of experiments and obtained two values of the Rabi frequency in the center of the DRA, 7.8 MHz and 7.4 MHz, as shown in Figs. 8(a) and 8(b), respectively. This slight disagreement can be explained by the scanning time. In fact, the scan of the Rabi frequency distribution map was performed over 23 h.

The main performances of the DRA design have been summarized in Table I together with the performances of other known antenna designs. We indicate the type of antennas' polarization, the level of input power, and the corresponding Rabi frequency. We also compare the bandwidth of the antenna design and demonstrate the diamond sample dimensions. However, not all the cited papers contain the information about the inhomogeneity of the field. We found these numbers only for several designs. However, we list them in the table to provide a qualitative comparison.

IV. CONCLUSION

We proposed a circularly polarized microwave antenna for the coherent manipulation of NV centers in a diamond. Circular polarization of the MW magnetic field was achieved by the excitation of two orthogonal $HEM_{11\delta}$ modes inside a high-permittivity microwave resonator. A numerical study of the mean value and inhomogeneity of the Rabi frequency was performed for various geometries of the resonator. For the geometry with $2R \approx T$, the mean value of the Rabi frequency of 34 MHz and inhomogeneity of 4% were achieved for a diamond volume of 1.2 mm × 02.5 mm under 10 W of total input power. The $2R \ll T$ resonator geometry provided a mean Rabi frequency of 20 MHz with 1% inhomogeneity, while the resonator geometry $2R \gg T$ provided a mean Rabi frequency value of 14.5 MHz with 6% homogeneity over the same diamond volume.

A DRA prototype was fabricated and experimentally studied. The DRA provided the circular polarization of the MW magnetic field with an ellipticity of 0.94. A maximum Rabi frequency of 7.8 MHz was achieved at a MW frequency of 2.67 GHz under 4 W of input power. The measured bandwidth of the resonance peak was 140 MHz. The measured mean value of the Rabi frequency deviated from the numerically obtained results by less than 0.6%, thus, confirming the calculations. While the current design of the antenna is a fixed frequency one, it could be extended to a tunable version. One approach would be to tune the resonant frequency of the DRA antenna mechanically, i.e., through adjusting stubs incorporated into excitation networks.[26] The other approach could be to use electrically tunable impedance matching networks based on variable capacitors.[37]

We believe that the proposed DRA design will find applications in the control and manipulation of quantum systems with a circularly polarized MW magnetic field over a large volume; an example is the uniform control of 3D and 2D spin ensembles of NV centers in ⟨111⟩-cut diamond samples for applications in ensemble sensing and wide-field magnetometry. The ability to control the polarization of the drive could become beneficial for driving the spin transition more efficiently with the available power and also for performing spin-selective transitions when multiple transitions coincide at the same frequency, such as in zero-field NMR.

ACKNOWLEDGMENTS

This work was supported by the Russian Science Foundation (Grant No. 19-19-00693).

REFERENCES

[1] J. F. Barry, M. J. Turner, J. M. Schloss, D. R. Glenn, Y. Song, M. D. Lukin, H. Park, and R. L. Walsworth, "Optical magnetic detection of single-neuron action potentials using quantum defects in diamond," Proc. Natl. Acad. Sci. U. S. A. **113**, 14133–14138 (2016).

[2] I. V. Fedotov, N. A. Safronov, Y. G. Ermakova, M. E. Matlashov, D. A. Sidorov-Biryukov, A. B. Fedotov, V. V. Belousov, and A. M. Zheltikov, "Fiber-optic control and thermometry of single-cell thermosensation logic," Sci. Rep. **5**, 15737 (2015).

[3] S. Ahmadi, H. A. R. El-Ella, A. M. Wojciechowski, T. Gehring, J. O. B. Hansen, A. Huck, and U. L. Andersen, "Nitrogen-vacancy ensemble magnetometry based on pump absorption," Phys. Rev. B **97**, 024105 (2018).

[4] T. Wolf, P. Neumann, K. Nakamura, H. Sumiya, T. Ohshima, J. Isoya, and J. Wrachtrup, "Subpicotesla diamond magnetometry," Phys. Rev. X **5**, 041001 (2015).

[5] V. M. Acosta, E. Bauch, M. P. Ledbetter, C. Santori, K.-M. C. Fu, P. E. Barclay, R. G. Beausoleil, H. Linget, J. F. Roch, F. Treussart, S. Chemerisov, W. Gawlik, and D. Budker, "Diamonds with a high density of nitrogen-vacancy centers for magnetometry applications," Phys. Rev. B **80**, 115202 (2009).

[6] C. S. Shin, C. E. Avalos, M. C. Butler, H.-J. Wang, S. J. Seltzer, R.-B. Liu, A. Pines, and V. S. Bajaj, "Suppression of electron spin decoherence of the diamond NV center by a transverse magnetic field," Phys. Rev. B **88**, 161412 (2013).

[7] E. R. Eisenach, J. F. Barry, L. M. Pham, R. G. Rojas, D. R. Englund, and D. A. Braje, "Broadband loop gap resonator for nitrogen vacancy centers in diamond," Rev. Sci. Instrum. **89**, 094705 (2018).

[8] P. Kapitanova, V. V. Soshenko, V. V. Vorobyov, D. Dobrykh, S. V. Bolshedvorskii, V. N. Sorokin, and A. V. Akimov, "3D uniform manipulation of NV centers in diamond using a dielectric resonator antenna," JETP Lett. **108**, 588–595 (2018).

[9] L. M. Pham, N. Bar-Gill, D. Le Sage, C. Belthangady, A. Stacey, M. Markham, D. J. Twitchen, M. D. Lukin, and R. L. Walsworth, "Enhanced metrology using preferential orientation of nitrogen-vacancy centers in diamond," Phys. Rev. B **86**, 121202 (2012).

[10] C. Osterkamp, M. Mangold, J. Lang, P. Balasubramanian, T. Teraji, B. Naydenov, and F. Jelezko, "Engineering preferentially-aligned nitrogen-vacancy centre ensembles in CVD grown diamond," Sci. Rep. **9**, 5786 (2019).

[11] G. Kukucska, V. Zólyomi, and J. Koltai, "Characterization of epitaxial silicene with Raman spectroscopy," Phys. Rev. B **98**, 075437 (2018).

[12] J. Michl, T. Teraji, S. Zaiser, I. Jakobi, G. Waldherr, F. Dolde, P. Neumann, M. W. Doherty, N. B. Manson, J. Isoya, and J. Wrachtrup, "Perfect alignment and preferential orientation of nitrogen-vacancy centers during chemical vapor deposition diamond growth on (111) surfaces," Appl. Phys. Lett. **104**, 102407 (2014).

[13] T. Fukui, Y. Doi, T. Miyazaki, Y. Miyamoto, H. Kato, T. Matsumoto, T. Makino, S. Yamasaki, R. Morimoto, N. Tokuda, M. Hatano, Y. Sakagawa, H. Morishita, T. Tashima, S. Miwa, Y. Suzuki, and N. Mizuochi, "Perfect selective alignment of nitrogen-vacancy centers in diamond," Appl. Phys. Express **7**, 055201 (2014).

[14] H. Ishiwata, M. Nakajima, K. Tahara, H. Ozawa, T. Iwasaki, and M. Hatano, "Perfectly aligned shallow ensemble nitrogen-vacancy centers in (111) diamond," Appl. Phys. Lett. **111**, 043103 (2017).

[15] H. Clevenson, M. E. Trusheim, C. Teale, T. Schröder, D. Braje, and D. Englund, "Broadband magnetometry and temperature sensing with a light-trapping diamond waveguide," Nat. Phys. **11**, 393–397 (2015).

[16] L. T. Hall, G. C. G. Beart, E. A. Thomas, D. A. Simpson, L. P. McGuinness, J. H. Cole, J. H. Manton, R. E. Scholten, F. Jelezko, J. Wrachtrup, S. Petrou, and L. C.

L. Hollenberg, "High spatial and temporal resolution wide-field imaging of neuron activity using quantum NV-diamond," Sci. Rep. **2**, 401 (2012).
[17]D. Le Sage, L. M. Pham, N. Bar-Gill, C. Belthangady, M. D. Lukin, A. Yacoby, and R. L. Walsworth, "Efficient photon detection from color centers in a diamond optical waveguide," Phys. Rev. B **85**, 121202 (2012).
[18]H. Zheng, J. Xu, G. Z. Iwata, T. Lenz, J. Michl, B. Yavkin, K. Nakamura, H. Sumiya, T. Ohshima, J. Isoya, J. Wrachtrup, A. Wickenbrock, and D. Budker, "Zero-field magnetometry based on nitrogen-vacancy ensembles in diamond," Phys. Rev. Appl. **11**, 064068 (2019).
[19]J.-P. Tetienne, T. Hingant, L. Rondin, S. Rohart, A. Thiaville, J.-F. Roch, and V. Jacques, "Quantitative stray field imaging of a magnetic vortex core," Phys. Rev. B **88**, 214408 (2013).
[20]K. Bayat, J. Choy, M. Farrokh Baroughi, S. Meesala, and M. Loncar, "Efficient, uniform, and large area microwave magnetic coupling to NV centers in diamond using double split-ring resonators," Nano Lett. **14**, 1208–1213 (2014).
[21]K. Sasaki, Y. Monnai, S. Saijo, R. Fujita, H. Watanabe, J. Ishi-Hayase, K. M. Itoh, and E. Abe, "Broadband, large-area microwave antenna for optically detected magnetic resonance of nitrogen-vacancy centers in diamond," Rev. Sci. Instrum. **87**, 053904 (2016).
[22]M. Mrózek, J. Mlynarczyk, D. S. Rudnicki, and W. Gawlik, "Circularly polarized microwaves for magnetic resonance study in the GHz range: Application to nitrogen-vacancy in diamonds," Appl. Phys. Lett. **107**, 013505 (2015).
[23]J.-M. Le Floch, N. Delhote, M. Aubourg, V. Madrangeas, D. Cros, S. Castelletto, and M. E. Tobar, "Towards achieving strong coupling in three-dimensional-cavity with solid state spin resonance," J. Appl. Phys. **119**, 153901 (2016).
[24]V. Yaroshenko, A. Zalogina, D. Zuev, P. Kapitanova, and I. Shadrivov, "Circularly polarized antenna for coherent manipulation of NV-centers in diamond," J. Phys.: Conf. Ser. **1092**, 012168 (2018).
[25]A. Angerer, T. Astner, D. Wirtitsch, H. Sumiya, S. Onoda, J. Isoya, S. Putz, and J. Majer, "Collective strong coupling with homogeneous Rabi frequencies using a 3D lumped element microwave resonator," Appl. Phys. Lett. **109**, 033508 (2016).
[26]C. A. Balanis, *Antenna Theory: Analysis and Design*, 4th ed. (John Wiley and Sons, Inc., 2016).
[27]K. M. Luk and K. W. Leung, *Dielectric Resonator Antennas*, 1st ed. (Research Studies Pr Ltd., 2002).
[28]J. Breeze, *Temperature and Frequency Dependence of Complex Permittivity in Metal Oxide Dielectrics: Theory, Modelling and Measurement* (Springer International Publishing, 2016).
[29]E. Nenasheva, N. Kartenko, I. Gaidamaka, O. Trubitsyna, S. Redozubov, A. Dedyke, and A. Kanareykin, J. Eur. Ceram. Soc. **30**, 395–400 (2010).
[30]J. Herrmann, M. A. Appleton, K. Sasaki, Y. Monnai, T. Teraji, K. M. Itoh, and E. Abe, "Polarization- and frequency-tunable microwave circuit for selective excitation of nitrogen-vacancy spins in diamond," Appl. Phys. Lett. **109**, 183111 (2016).
[31]M. O. Scully and M. S. Zubairy, *Quantum Optics* (Cambridge University Press, 1997), p. 152.
[32]N. Zhang, H. Yuan, C. Zhang, L. Xu, J. Zhang, G. Bian, P. Fan, H. Yuan, and J. Fang, "Microwave field uniformity impact on DC magnetic sensing with NV ensembles in diamond," IEEE Sens. J. **19**, 451–456 (2019).
[33]L. F. Chen, C. K. Ong, C. P. Neo, V. V. Varadan, and V. K. Varadan, *Microwave Electronics: Measurement and Materials Characterization* (Wiley-Blackwell, 2005).
[34]I. V. Kotel'nikov, V. N. Osadchii, D. M. Kos'min, A. D. Kanareikin, E. A. Nenasheva, and A. B. Kozyrev, "Method and apparatus for measuring the microwave parameters of nonlinear ceramics in control electric fields," Meas. Tech. **57**, 1077–1081 (2014).
[35]P. Kapitanova, V. V. Soshenko, V. V. Vorobyov, V. Yaroshenko, S. V. Bolshedvorsky, V. Sorokin, and A. Akimov, "Efficient, uniform, and large-volume microwave magnetic coupling to NV centers in diamond using dielectric resonator antennas," Proc. SPIE **10733**, 1073306 (2018).
[36]O. R. Rubinas, V. V. Vorobyov, V. V. Soshenko, S. V. Bolshedvorskii, V. N. Sorokin, A. N. Smolyaninov, V. G. Vins, A. P. Yelisseyev, and A. V. Akimov, "Spin properties of NV centers in high-pressure, high-temperature grown diamond," J. Phys. Commun. **2**, 115003 (2018).
[37]S. A. Aussenhofer and A. G. Webb, "Design and evaluation of a detunable water-based quadrature HEM11 mode dielectric resonator as a new type of volume coil for high field MRI," Magn. Reson. Med. **68**, 1325–1331 (2012).